CORE
Metadata, citation and similar papers at core.ac.uk
Provided by Open Archive Toulouse Archive Ouverte

Open Archive TOULOUSE Archive Ouverte (OATAO)
OATAO is an open access repository that collects the work of Toulouse researchers and makes it freely available over the web where possible.

This is an author-deposited version published in: http://oatao.univ-toulouse.fr/
Eprints ID: 19367

To link to this article: DOI: 10.1016/j.ces.2017.12.006
URL: http://dx.doi.org/10.1016/j.ces.2017.12.006

To cite this version: Psarellis, George M. and Aviziotis, Ioannis G. and Duguet, Thomas and Vahlas, Constantin and Koronaki, Eleni D. and Boudouvis, Andreas G. *Investigation of reaction mechanisms in the chemical vapor deposition of al from DMEAA*. (2018) Chemical Engineering Science, vol. 177. pp. 464-470. ISSN 0009-2509

Any correspondence concerning this service should be sent to the repository administrator: staff-oatao@listes-diff.inp-toulouse.fr

Investigation of reaction mechanisms in the chemical vapor deposition of al from DMEAA

George M. Psarellis [a], Ioannis G. Aviziotis [a,b,*], Thomas Duguet [b], Constantin Vahlas [b], Eleni D. Koronaki [a], Andreas G. Boudouvis [a]

[a] School of Chemical Engineering, National Technical University of Athens, Heroon Polytechniou 9, 15780 Zografou, Greece
[b] CIRIMAT, CNRS, Université de Toulouse, 4 alleé Emile Monso, BP 44362, 31030 Toulouse cedex 4, France

HIGHLIGHTS

- Experimental and computational analysis of Al CVD from DMEAA.
- Detailed chemistry mechanism with side reactions.
- AlH_3 gas phase oligomerization and surface dehydrogenation steps.
- Prediction of experimentally measured deposition rate.
- Decrease of deposition rate due to AlH_3 oligomerization and surface desorption.

ABSTRACT

We propose a novel reaction scheme for the chemical vapor deposition (CVD) of Al films on substrates from dimethylethylamine alane (DMEAA), supported by the prediction of the Al deposition rate as a function of process temperature. The scheme is based on gas phase oligomerizations of alane which form a substantial amount of intermediates. Combined with reversible surface dehydrogenation steps, the global deposition reaction is composed of a set of 12 chemical reactions. This new scheme entails four intermediates and includes side reactions that play an important role in the formation of Al thin films. The chemistry mechanism is incorporated in a 2D Computational Fluid Dynamics (CFD) model of the CVD reactor setup used for the experimental investigation. The simulation predictions of the Al deposition rate are in good agreement with corresponding experimental measurements. The success of this novel reaction pathway lies in its ability to capture the abrupt decrease of the deposition rate at temperatures above 200 °C, which is attributed to the gas phase consumption of alane along with its increased desorption rate from the film surface.

Keywords:
Modeling aluminum CVD
Reaction mechanisms
Alane oligomerization
Alane dehydrogenation
Surface desorption
Surface site reactions

1. Introduction

Thin aluminum (Al) solid films show advantageous properties, such as high electrical conductivity (Lee et al., 2014) and significant resistance to electromigration (Tan and Roy, 2007) and corrosion (Hamasha et al., 2011) rendering them ideal constituents for integrated circuits. Moreover, Al can be applied as component in metallic alloys, such as $AlFe_3$ (Sundman et al., 2009), $AlPt_3$ (Delmas et al., 2005) or $Al_{13}Fe_4$ (Armbrüster et al., 2012) to provide advanced materials with enhanced mechanical and thermal properties, catalytic activity and wetting properties, respectively. Chemical vapor deposition (CVD) of Al has been applied for the industrial production of wires, multilevel interconnections of ultra large scale integrated circuits (ULSI) (Yun et al., 1998a; Masu et al., 1994), micro-plugs and electric interconnects (Amazawa et al., 1998) and for the processing of films composed of the approximant γ-Al_4Cu_9 (Aloui et al., 2012).

Compared to other deposition techniques, such as PVD, magnetron sputtering or ALD, CVD combines high throughput, versatility, successful control of the film microstructural characteristics and most importantly the conformal coverage of non-line-of-sight surfaces (Kleijn et al., 2007; Vahlas, 2010).

In order to control the process and achieve the maximum potential, the chemical mechanisms as well as the transport phenomena occurring in the CVD reactor have to be investigated and

* Corresponding author at: School of Chemical Engineering, National Technical University of Athens, Heroon Polytechniou 9, 15780 Zografou, Greece.
E-mail address: javiziot@chemeng.ntua.gr (I.G. Aviziotis).

https://doi.org/10.1016/j.ces.2017.12.006

understood (Aviziotis, 2016). In particular, it is suggested that detailed reaction pathways have to be considered instead of reduced schemes, since various intermediates can play a significant role in the overall deposition process (Aviziotis et al., 2017; Kuwana et al., 2006; Kleijn, 2000). Despite such well admitted requirements, limited research is available on the detailed chemistry scheme of Al-CVD using a DMEAA (dimethylethylamine alane) precursor; i.e., a commonly used precursor, allowing processing of pure Al films at low temperature (Simmonds et al., 1994; Luo and Gladfelter, 2009).

Several studies have been reported dealing with the deposition behavior and chemistry mechanisms of DMEAA on the surface. Han et al. (1994) proposed that the rate limiting step is either the decomposition of DMEAA on the surface of the substrate or the desorption of the molecular hydrogen from the surface, or a combination of these two reaction steps. Furthermore, Kim et al. (1996), suggested that DMEAA may dissociate in the gas phase, at temperature values higher than 170 °C leading to the formation of powders.

DMEAA may also decompose in the gas phase. Yun et al. (1998b) reported the value of the activation energy of this gas phase decomposition by performing FTIR analysis of the gas phase. They also confirmed the formation of powder at elevated temperature as a result of oligomerization reactions that AlH_3 may undergo in the gas phase. Finally, the experimental data reported in the literature (Aviziotis et al., 2015; Jang et al., 1998; Kim et al., 1996; Yun et al., 1998a, 1998b) show that the Al deposition rate decreases considerably above 200 °C. Hypotheses have been formulated to explain this behavior including the increased gas phase dissociation rate of DMEAA as a competitive mechanism to the deposition process (Kim et al., 1996), the increased desorption rate of the precursor (Choy, 2003) or the recombinative desorption of H_2 from the monohydride adsorbate H_{ads} which occurs at high temperature on Si(1 0 0) (Robinson and Rogers, 2000).

Nakajima et al. (2003) performed quantum chemical calculations to determine the mechanisms occurring on the surface during the process. They suggested that the precursor is adsorbed on the surface where it dissociates to AlH_3 and DMEA. DMEA is rapidly desorbed from the surface whereas AlH_3 undergoes several dehydrogenation steps before the deposition of atomic Al. The above-mentioned report does not consider reactions in the gas phase although they can have a significant effect on the Al deposition rate.

In previous works (Xenidou et al., 2007, 2010), it was suggested that one gas phase and one surface reaction can capture the deposition of Al films. These reactions involve the gas phase and the surface dissociation of DMEAA, as follows:

$$DMEAA_{(g)} \rightarrow DMEA_{(g)} + AlH_{3(g)} \tag{1}$$

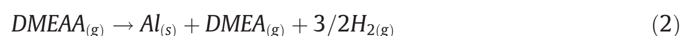

$$DMEAA_{(g)} \rightarrow Al_{(s)} + DMEA_{(g)} + 3/2H_{2(g)} \tag{2}$$

Although deposition profiles on substrates correlate satisfactorily with the experimental data, the behavior of the deposition rate as a function of the substrate's temperature is investigated at only four different temperature values. Hence, there is limited data to extract useful information concerning the reaction mechanisms of the process. Recently, we have reported a combined experimental and computational study (Aviziotis et al., 2015) for the investigation of the average deposition rate as a function of the surface temperature, in a more detailed temperature range. By incorporating the reaction scheme of Eqs. (1) and (2) into the computational model, we managed to predict satisfactorily the deposition rate at the low temperature regime but not at higher temperature. We have deduced that the chemistry scheme that consists of the above-mentioned reactions along with first-order Arrhenius type kinetics do not predict with sufficient accuracy the experimental data, especially at temperatures higher than 200 °C. Thus, a more detailed chemistry pathway is required with the corresponding kinetic mechanisms for the description of the phenomena occurring at higher temperatures.

The present work provides a combined experimental and theoretical investigation of the deposition of Al from DMEAA. A two-dimensional (2D) macroscopic model is developed based on first principles, i.e., the conservation of mass, momentum and energy, and it accounts for transport mechanisms in the bulk of the CVD reactor. In addition, the macroscopic model includes for the first time a detailed chemistry model based on comprehensive literature information and describes the gas phase and the surface reactions of the precursor and pertinent. The predictive capability of the model is validated through the comparison of the theoretical output with corresponding experimental measurements, namely with the deposition rate determined as a function of the deposition temperature.

2. Experimental

Deposition of Al films is performed in a vertical, cylindrical, stagnant flow, warm wall, stainless steel MOCVD reactor which has been described in detail in Xenidou et al. (2010). The preparation of the silicon (Si) coupons used as substrates supported on a susceptor is described in our previous work (Aviziotis et al., 2015). DMEAA is synthesized by NanoMePS[1] and is supplied in a stainless steel bubbler equipped with a 3-valve bypass system. It is maintained at 3 °C permanently; i.e. below the freezing point of the compound, thus strongly limiting its degradation (Matsuhashi et al., 1999). It is thermally regulated to 7 °C during the experiments. At this temperature, the partial pressure of DMEAA is 0.7 Torr (Frigo et al., 1994). Pure nitrogen (99.998%, Air Products) is fed through computer-driven mass flow controllers (MKS).

Experiments are performed at fixed conditions, namely total pressure of the reactor P_{tot} = 10 Torr, thermal regulation of the lines T_{lines} = 100 °C and of the walls of the reactor T_{walls} = 75 °C, while the N_2 dilution gas flow ($Q_{N2,dilution}$) and the N_2 carrier gas flow through the precursor ($Q_{N2,prec}$) equal 305 and 25 standard cubic centimeters per minute (sccm), respectively. Considering the relation proposed by Hersee and Ballingal (1990), these conditions yield a maximum flow rate Q_{prec} of DMEAA in the input gas, equal to 2 sccm. However, as we have shown in Aviziotis et al. (2015), the effective mass inflow rate of the precursor equals 1.85 sccm. A perforated plate (shower plate), located above the susceptor, enhances the entering gas distribution and mixing.

Independent experiments are performed at eight different substrate temperature values, T_s, in the range 139–241 °C. T_s was calibrated under rough vacuum by attaching a thermocouple to the surface of a dummy Si coupon. The deposition time is 1 h in all experiments, including the time required for the nucleation to take place at each T_s, that is the incubation time. We have referred in detail to the importance of the incubation time for the determination of net deposition rate in Aviziotis et al. (2015). The deposition rate is evaluated directly by weight difference (±10 µg) of the substrates before and after deposition, using a microbalance (Sartorius).

The microstructural characteristics of the films such as morphological observations of the surface and the determination of the surface roughness both experimentally and computationally have been reported in our previous works (Aviziotis et al., 2015, 2016) and it is not a matter of investigation in the present work.

[1] www.nanomeps.fr, last visited July 5, 2017.

3. Process modeling – Chemistry mechanism

For the investigation of the chemistry pathway and the kinetic mechanisms of Al films growth, a 2D model of the MOCVD reactor is built, based on the governing equations describing the transport phenomena and the chemical reactions inside the reactor. The reactor model is presented in Fig. 1 to assist the reader on the identification of various part discussed in the next section. The continuity, momentum, energy and the species transport equations augmented with realistic boundary conditions (Cheimarios et al., 2010; Deen, 1998) are discretized with the finite volume method and the resulting system of equations is solved with Ansys/Fluent (Ansys/Fluent, 2009).

3.1. Gas phase reactions and kinetics

DMEAA can be easily decomposed in the gas phase, as it is indicated by its low decomposition energy compared to other gas phase reactions, as shown in Table 1 (Xenidou et al., 2010; Yun et al., 1998b). The products of this decomposition are DMEA and AlH_3. It is known and accounted for in this work that metal hydrides such as AlH_3 can form polymers at high temperature (Aitken and Harrod, 1985; Kawamura et al., 2003; Michos et al., 2016). Kawamura et al. (2003) investigated the gas phase polymerization of alane and studied the kinetics of the dimerization, trimerization and other related oligomer producing reactions (oligomers with 2–7 Al atoms) both linear and cyclic. They calculated the activation energies and the pre-exponential factors by employing first-principles calculations with a plane-wave basis and a method of a linear combination of atomic-orbitals. Our model accounts only for the dimerization and trimerization reactions, since we aim at incorporating a mechanism of depletion of AlH_3 and not the polymerization process of this compound *per se*.

The gas phase reactions (G1–G3) with their corresponding energies are summarized in Table 1. For this scheme, we modify the Arrhenius law implemented in Fluent (Ansys/Fluent 2009) to account for the stoichiometry of the reactions. The Arrhenius reaction rate corresponding to these reactions is:

$$R_{G_i} = k_{0,G_i} \exp\left(-\frac{E_{a,G_i}}{RT_{gas}}\right)\Pi C_i^n, \quad (3)$$

where R_{G_i} denotes the reaction identity, C_i^n the gas phase concentration of the corresponding species, i and the order of the reaction, n, E_{a,G_i} is the activation energy and T_{gas} is the temperature of the gas phase in the reactor. The pre-exponential factor, k_{0,G_i}, of the first reaction is provided by Yun et al. (1998b). The pre-exponential factors of the two other reactions are fitted to the experimental data. In order to fit the unknown pre-exponential factors of the gas-phase reactions, the process is simulated first at the high-temperature regime, where the gas phase reaction rates are high and gas phase processes become dominant for the deposition process. The pre-exponential factors fitted in the diffusion-limited regime are applied for the simulation of the process in the whole temperature range for a fine tuning. Values of the pre-exponential factors for each reaction are summarized in Table 1.

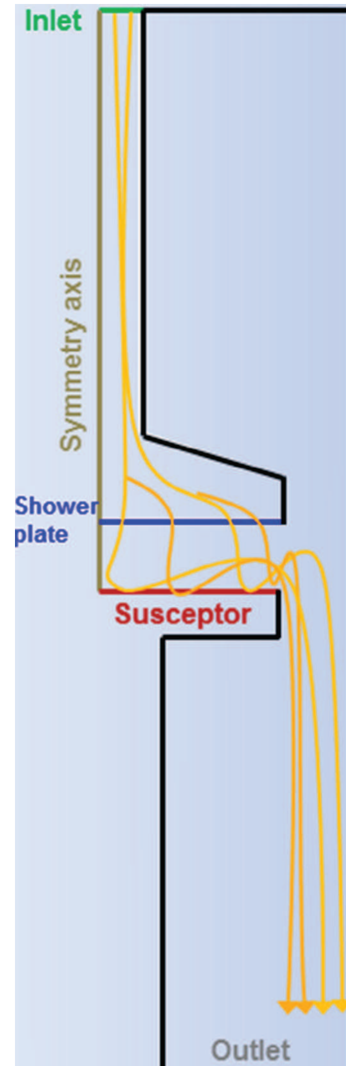

Fig. 1. The 2D geometry of the reactor built for the simulation of the CVD of Al.

As indicated in Table 1, the oligomerization reactions (G2–G3) have much higher activation energies than the decomposition of the precursor (G1). This would explain the activation of these reactions at high temperature with a subsequent consumption of AlH_3 prior reaching the deposition surface.

3.2. Surface reactions

The surface reaction pathway that we propose is similar to the one reported by Nakajima et al. (2003). The AlH_3 which does not

Table 1
The gas phase reaction scheme of the CVD of Al from DMEAA. The Arrhenius rate expressions are given by Eq. (3).

ID	Reaction	Pre-exponential factor	Activation energy (kJ mol^{-1})
G1	DMEAA → DMEA + AlH_3	2.0×10^7 s^{-1} [a]	40.06[a]
G2	$2AlH_3 \rightarrow Al_2H_6$	2.55×10^{20} m^3 $kmol^{-1}$ s^{-1} [b]	118.0[c]
G3	$AlH_3 + Al_2H_6 \rightarrow Al_3H_9$	7.75×10^{20} m^3 $kmol^{-1}$ s^{-1} [b]	90.70[c]

[a] Yun et al. (1998b).
[b] This work.
[c] Kawamura et al. (2003).

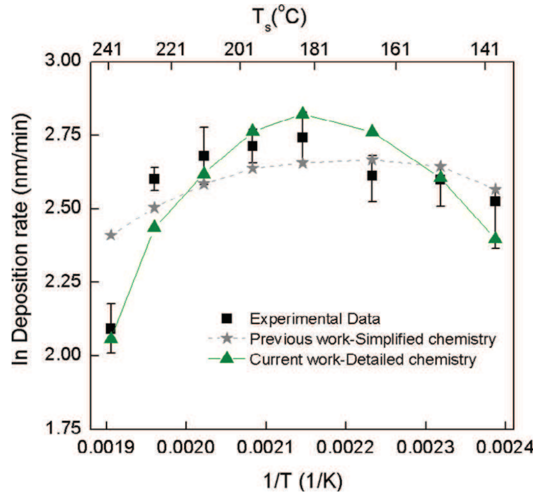

Fig. 2. The Arrhenius plot of the CVD of Al from DMEAA. Experimental measurements (squares) and computational predictions with the detailed (solid line with triangles) and the simplified (dashed line with stars) chemistry mechanisms are shown.

undergo gas phase oligomerization, reaches and is adsorbed on the heated surface. According to Nakajima et al. (2003), it occupies three surface sites during its adsorption, one for the Al atom itself and two for the H atoms. The third H atom is located above the Al atom in the opposite direction to the surface. This inverted tetrahedron structure of AlH_3 has been also reported by Chaudhuri et al. (2008). For the activation energy of the adsorption of AlH_3 on the surface we apply the value extracted from the experimental Arrhenius plot (see below Fig. 2) while for that of the AlH_3 desorption the value reported by Chaudhuri et al. (2008).

Once adsorbed on the surface, AlH_3 begins to undergo reversible dehydrogenation steps for the formation of AlH_2, AlH and eventually Al. The surface structures of AlH_2 and AlH are similar to that of AlH_3, i.e., they occupy two and one surface sites, respectively. The surface reactions with their corresponding activation energies are summarized in Table 2, where S denotes the unoccupied surface sites.

The surface decomposition of AlH_3 (SR2), its reverse reaction (SR3), the surface recombination of AlH with H (SR5) and the recombinative desorption of H (SR8) are rather easy due to their small activation energies. In contrast, the reaction resulting in the deposition of Al (SR7) seems more difficult to proceed since its activation energy is quite high compared to the other reactions.

As we briefly mention above, the surface processes of AlH_3 and its surface decomposition products involve their surface structures and the occupation of surface sites. That is, inhibition of surface availability due to the adsorbed species may occur during the process. For this reason, we implement a modified Arrhenius type expression:

$$R_{S_i} = k_{0,S_i} \exp\left(-\frac{E_{a,S_i}}{RT_s}\right) \Pi C_i^n, \tag{4}$$

Here R_{S_i} denotes the reaction identity, E_{a,S_i} is the activation energy of each reaction and T_s is the temperature of the substrate. The modification of this rate equation lies in the concentration term, C_i, which expresses the concentration of each adsorbed species as a function of the surface coverage and the site density:

$$C_i = \theta_i \times d, \tag{5}$$

where θ_i is the coverage of each adsorbed species and d is the site density in kmol m^{-2} as required by the computational software (Ansys/Fluent, 2009). For the site density we apply the value of 10^{-9} kmol m^{-2}, a value in the range of the one reported by Letterman and Iyer (1985).

The pre-exponential factors, k_{0,S_i}, are fitted to the experimental data. For the fitting of these parameters, the process is first simulated at the reaction-limited regime where surface reactions are more important than gas phase reactions or diffusion mechanisms. Then, simulations are performed in the whole temperature range for the better fitting of the pre-exponential factors. Exception to this process are reactions SR7 and SR9 which describe the desorption of H_{ads} and $AlH_{3,ads}$. Since desorption is favored at high temperature, the pre-exponential factors of these reactions are first fitted to the experimental data at the high temperature regime. It is noted here that Nakajima et al. (2003) determined the values of the pre-exponential factors of reactions SR2–SR5 and SR7–SR8 based on transition state theory calculations. Thus, these values correspond to vibrational frequencies (s-1) at the atomic scale. At the macroscopic level where we model the process, we apply apparent pre-exponential factors rather than vibrational frequencies. Thus, we fit these kinetic parameters instead of using the values reported by Nakajima et al. (2003). Nevertheless, we maintain unchanged the ratio of the pre-exponential factor of the forward reactions to that of the reverse reactions, for consistency to their work.

4. Results and discussion

Fig. 2 presents the Arrhenius plot of the process where both experimental measurements (squares) and computational predictions are shown. Error bars attached to the experimental results correspond to the minimum and the maximum deviations of the

Table 2
The surface reaction scheme of the CVD of Al from DMEAA. The kinetic expressions are given by Eq. (4). The units of the pre-exponential factors of each reaction are consistent with Fluent units (Ansys/Fluent 2009).

ID	Reaction	Pre-exponential factor	Activation energy (kJ mol^{-1})
SR1	$AlH_{3(g)} + 3S \rightarrow AlH_{3(ads)}$	4.42×10^{8} m s^{-1}[a]	19.68[b]
SR2	$AlH_{3(ads)} \rightarrow AlH_{2(ads)} + H_{(ads)}$	1.02×10^{12} m s^{-1}[a]	19.25[c]
SR3	$AlH_{2(ads)} + H_{(ads)} \rightarrow AlH_{3(ads)}$	5.11×10^{12} m^4 $kmol^{-1}$ s^{-1}[a]	18.41[c]
SR4	$AlH_{2(ads)} \rightarrow AlH_{(ads)} + H_{(ads)}$	4.98×10^{12} m s^{-1}[a]	37.43[c]
SR5	$AlH_{(ads)} + H_{(ads)} \rightarrow AlH_{2(ads)}$	1.05×10^{14} m^4 $kmol^{-1}$ s^{-1}[a]	8.37[c]
SR6	$AlH_{(ads)} \rightarrow Al_{(s)} + H_{(ads)}$	2.93×10^{10} m s^{-1}[a]	76.82[c]
SR7	$2H_{(ads)} \rightarrow H_{2(g)} + 2S$	5.50×10^{14} m^4 $kmol^{-1}$ s^{-1}[a]	12.55[c]
SR8	$H_{2(g)} + 2S \rightarrow 2H_{(ads)}$	3.07×10^{10} m s^{-1}[a]	76.97[c]
SR9	$AlH_{3(ads)} \rightarrow AlH_{3(g)} + 3S$	2.38×10^{16} m s^{-1}[a]	86.84[d]

[a] This work.
[b] Aviziotis et al. (2015) and this work.
[c] Nakajima et al. (2003).
[d] Chaudhuri et al. (2008).

deposition rate and include potential overestimations of the incubation time. The simulations performed with the detailed chemistry pathway proposed in this work correspond to the solid line with triangles. The results obtained by using the simplified chemistry mechanism (Aviziotis et al., 2015) are also presented (dashed line with stars) for comparison. Observations of the experimental results reveal that it is difficult to distinguish the reaction-limited regime from the diffusion-limited regime, and this has also been reported by Jang et al. (1998). Despite this ambiguous behavior, a trend corresponding to a reaction-limited regime can be identified up to 185 °C through the increase of the deposition rate up to this temperature, in good agreement with previous works (Jang et al., 1998; Yun et al., 1998a). There is a potential overestimation of the incubation time for the lowest T_s resulting in the overestimation of the growth rate at 130 °C (Aviziotis et al., 2015, 2017) and this accounts for the misfit between the simulated and the experimental results at this T_s. At temperature higher than 185 °C, the deposition rate slightly decreases prior to a steep reduction at the highest temperature of the investigated range and the process is controlled by transport and competitive phenomena which have been considered in the detailed model.

The computational predictions with the detailed chemistry mechanism show satisfactory agreement with the experimental data in the whole temperature range, since they lie within the experimental deviations. In particular, at low temperature the model predicts with sufficient accuracy the measured deposition rate, except the point corresponding at 167 °C, which is off the trend clearly defined from the experimental result. The deposition rate at higher temperature can also be predicted successfully, especially at the highest investigated temperature of 241 °C, which is the major improvement compared to the simplified model. At this temperature, the computational model is capable of predicting the steep decrease of the deposition rate accurately.

We now further explore the successful prediction of the behavior of the deposition rate. We compare the G1 gas phase reaction rate (Table 1) at two temperature values, 151 °C corresponding to the reaction-limited regime and 241 °C, where the abrupt decrease of the rate is observed.

Fig. 3 shows the gas phase decomposition rate of DMEAA (reaction G1) in the reactor at 151 °C (Fig. 3(a)) and at 241 °C (Fig. 3(b)). At the inlet of the reactor where the temperature is 100 °C, the decomposition of the precursor has already occurred. As the mixture moves within the tube the rate slightly decreases, since the temperature in this domain is lower. Before the exit from the shower plate, the values of the gas phase decomposition rate of the precursor for the two temperature values are similar. However, when the mixture approaches the susceptor, the decomposition rate increases as the temperature at this point of the reactor is higher. This increase is more pronounced at T_s = 241 °C (Fig. 3b).

The revealed elevated decomposition rate of DMEAA at 241 °C should lead to a higher concentration of AlH_3 between the shower head and the susceptor than at 151 °C. Fig. 4 presents the mass fraction of AlH_3 for these two temperature values in the reactor. Contrary to expectations, it can be seen that the concentration of AlH_3 is lower at T_s = 241 °C than that at 151 °C. Indeed, at the lowest deposition temperature the mass fraction of AlH_3 reaches its maximum value of 4.98×10^{-3} in the area enclosed by the showerhead and the susceptor. On the other hand, the corresponding value at 241 °C varies between 1.2×10^{-3} and 3.7×10^{-3}, when moving from the susceptor to the showerhead, respectively. That is, the available AlH_3 at the surface level is four time less at T_s = 241 °C.

Fig. 5 depicts the reaction rate of the AlH_3 dimerization (Reaction G2 – Table 2). This reaction requires high activation energy in order to occur and it is thus favored at high process temperature. This is confirmed in Fig. 5 which reveals that at 241 °C the reaction

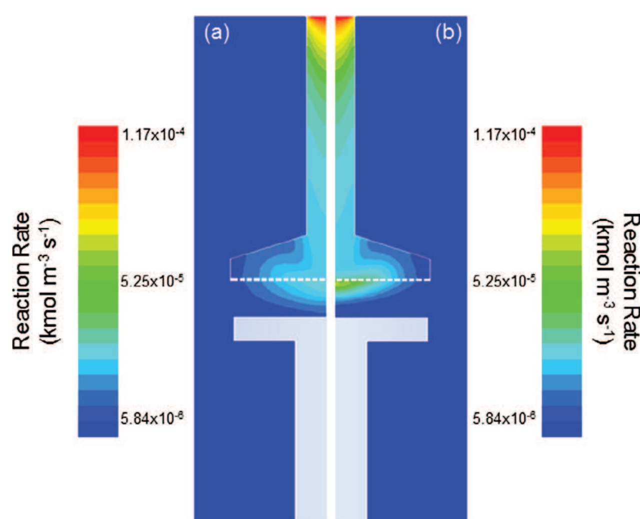

Fig. 3. The gas phase decomposition rate of DMEAA (Reaction G1 – Table 1) at (a) T_s = 151 °C and (b) T_s = 241 °C.

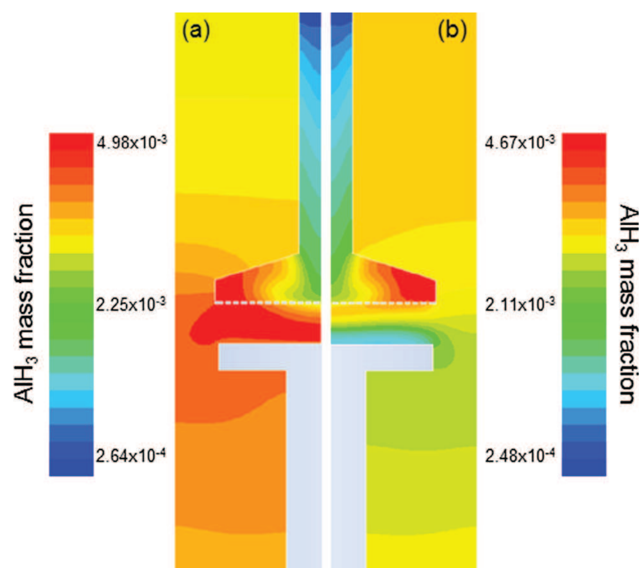

Fig. 4. The distribution of the AlH_3 mass fraction in the CVD reactor at (a) T_s = 151 °C and (b) T_s = 241 °C.

rate of G2 is twenty times higher than that at 151 °C. It should be noted that G2 occurs only close to the surface where the temperature is elevated. A direct conclusion of this discussion is that the oligomerization reactions of AlH_3, starting from G2, are activated at high temperatures. These reactions result in the depletion of AlH_3 in the gas phase. In turn, this impacts the surface processes and the deposition rate, since the consumed AlH_3 is not available to be adsorbed on the surface and activate the proposed surface reaction pathway for the deposition of Al.

In addition to the effect of the gas phase reactions on the process, we also examine the behavior of the surface processes as a function of the surface temperature. Fig. 6 shows in the form of histogram the rates of the surface reactions at T_s = 151 °C (simple column bars) and T_s = 241 °C (pattern column bars). The two histograms include only reactions that have measurable rates and not reactions which give negligible or zero rates. It is observed that forward reactions have higher rates than the corresponding reverse reactions and consequently, the deposition of Al is feasible.

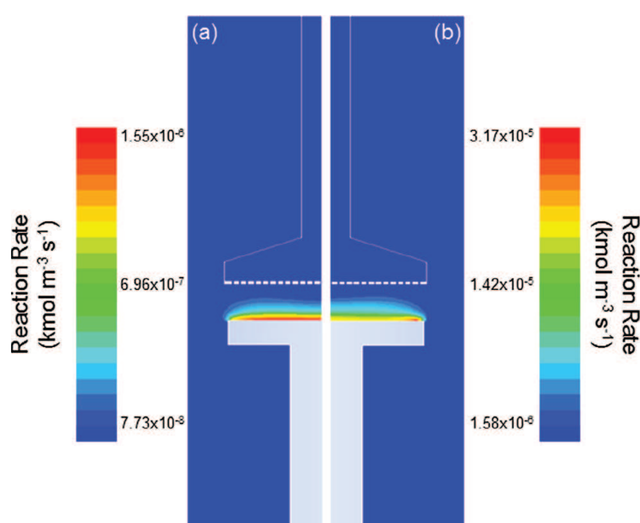

Fig. 5. The gas phase dimerization rate of AlH_3 (Reaction 2 – Table 1) at (a) T_s = 151 °C and (b) T_s = 241 °C.

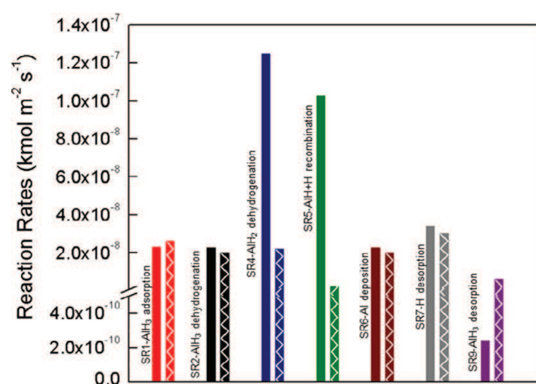

Fig. 6. The surface reactions rates as extracted from the computations with the proposed chemistry scheme at T_s = 151 °C and T_s = 241 °C. Simple column bars correspond to the former T_s whereas patterned column bars to the latter.

At low temperature, the reactions which describe the decomposition of AlH_2 to AlH and H and the reverse process (SR4 (blue) and SR5 (green) – Table 2) have significantly higher rates than the rest of the surface reactions. This can be attributed both to the abundance of reactants for these reactions and to their thermodynamic advantage due to their kinetic parameters. Furthermore, the rates of AlH_3 adsorption (SR1 (red) – Table 2), AlH_3 decomposition (SR2 (black) – Table 2) and H desorption (SR7 (grey) – Table 2) seem to be similar for both T_s, while the re-adsorption of H_2 on the surface appears to be negligible.

However, the major finding in Fig. 6 is that the rate of desorption of alane (SR9 (purple) – Table 2) is approximately thirty times higher at the high T_s compared to the corresponding rate at T_s = 151 °C. In particular, the reaction rate at T_s = 241 °C is 6.3×10^{-9} kmol m^{-2} s^{-1}, while at T_s = 151 °C is 2.2×10^{-10} kmol m^{-2} s^{-1}. It is this increase of the AlH_3 desorption which contributes significantly to the steep reduction of the Al deposition rate at high temperature. That is, at high temperature the increased AlH_3 desorption renders it unavailable for the surface processes and eventually, the deposition rate decreases.

We further investigate the surface composition through the amount of each intermediate species. Fig. 7 presents the surface coverage of AlH_3, AlH_2, AlH and H as well as the unoccupied Al surface sites in the form of logarithmic scale histogram at T_s = 151 °C

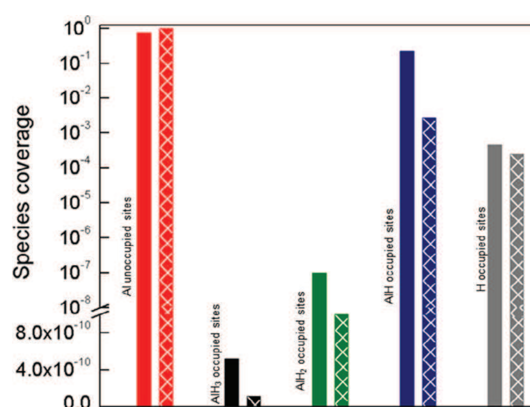

Fig. 7. The surface coverage of Al, AlH_3, AlH_2, AlH and H at T_s = 151 °C and T_s = 241 °C. Simple column bars correspond to the former T_s whereas patterned column bars to the latter.

(simple column bars) and at T_s = 241 °C (pattern column bars). It can be seen that the surface coverage varies with T_s. In particular, at 151 °C the bare Al unoccupied surface sites represent approximately 77.5% of the total surface sites. The rest of the surface sites are occupied mainly by the intermediate AlH (≈22.5%) and by a small amount of atomic H (0.05%). The surface coverage of the remaining species, AlH_3 and AlH_2, is negligible. On the other hand, at 241 °C the bare Al unoccupied surface sites almost represent the whole surface (99%), and the adsorbed species follow the same order as before (AlH > H > AlH_3 > AlH_2). The difference in the percentage of the unoccupied Al surface sites between the two T_s can be explained as before by the elevated desorption rates which have the same order of magnitude as the adsorption rates. The higher amount of AlH at the surface compared to the other intermediate species is consistent with literature findings (Nakajima et al., 2003).

5. Conclusions

Chemical vapor deposition of aluminum films from dimethylethylamine alane is investigated with the aim to understand and control the Al deposition rate at surface temperature in the range 139–241 °C. To meet this objective, we propose a new chemistry pathway for the process based on our combined experimental and computational findings and previous published results.

The Arrhenius plot of the process reveals two regimes; the reaction-limited regime, where the Al deposition rate increases with temperature, prevails within the temperature range 139–185 °C. At the latter temperature the deposition rate reaches its maximum value and above this temperature starts decreasing. At the highest investigated temperature, the Al deposition rate decreases abruptly due to the increased desorption from the surface and the prevailing of gas phase oligomerization reactions. The macroscopic computational model including the proposed chemistry mechanisms of the process (3 gas phase reactions and 9 surface processes) predicts the deposition rate in the examined temperature range with sufficient accuracy, especially at the highest temperature where previous models have failed.

The model reveals that the decrease of the Al deposition rate at high temperature is attributed to the activation of oligomerization reactions of AlH_3 which is depleted in the gas phase. As a result, AlH_3 is not available for surface reactions and the deposition rate decreases. Furthermore, by studying the dependence of the surface reactions on the temperature, it is observed that the increased AlH_3 desorption rate at high temperature results in the decrease of the

Al deposition rate. Taking into account that the dimerization rate of AlH_3 is four orders of magnitude higher than the corresponding desorption rate of AlH_3 from the surface, the primary cause of the abrupt decrease of the deposition rate at higher temperature is the activation of AlH_3 oligomerization reactions. However, surface desorption of AlH_3 contributes also to the reduction of the Al deposition rate. Thus, the computational model reveals the two main reasons for the reduction of the deposition rate at high temperature.

Acknowledgements

I.G.A. acknowledges the financial support provided by the National Scholarship Foundation of Greece (IKY-Siemens Program, Grant number: #SpnD/11160/13β). Partial funding was provided the Institut Français du Petrole et des Energies Nouvelles (IFPEN through the contract #268821, and support by the European Integrated Center for the Development of New Metallic Alloys and Compounds (C-MAC) for support. Marius Ozenil, student at the University of Vienna, contributed to this work during his summer 2016 internship at the National Technical University of Athens.

References

Aitken, C., Harrod, J.F., 1985. Alkyl dichloroacetates: a novel application in the preparation of highly functionalised aziridines from imines. J. Organomet. Chem. 280, C11–C13.

Aloui, L., Duguet, T., Haidara, F., Record, M.-C., Samélor, D., Senocq, F., Mangelinck, D., Vahlas, C., 2012. Al-Cu intermetallic coatings processed by sequential metalorganic chemical vapor deposition and post deposition annealing. Appl. Surf. Sci. 258, 73–80.

Amazawa, T., Yamamoto, T., Arita, Y., 1998. Planarized multilevel interconnection using chemical mechanical polishing of selective CVD–Al via plugs. IEEE Trans. Electron Dev. 45, 815–820.

Ansys/Fluent v12.1sp1. Documentation. Ansys Inc., 2009.

Armbrüster, M., Konvir, K., Friedrich, M., Teschner, D., Wowsnick, G., Hahne, M., Gille, P., Szentmiklósi, L., Feuerbacher, M., Heggen, M., et al., 2012. $Al_{13}Fe_4$ as a low-cost alternative for palladium in heterogeneous hydrogenation. Nat. Mater. 11, 690–693.

Aviziotis, I.G., 2016. Chemical Vapor Deposition of Al, Fe and of the Al13Fe4 Approximant Intermetallic Phase: Experiments and Multiscale Simulations. Ph. D. Thesis, National Technical University of Athens, Greece.

Aviziotis, I.G., Duguet, T., Soussi, K., Kokkoris, G., Cheimarios, N., Vahlas, C., Boudouvis, A.G., 2015. Investigation of the kinetics of the chemical vapor deposition of aluminum from dimethylethylamine alane: experiments and computations. Phys. Status Solidi C 12, 923–930.

Aviziotis, I.G., Cheimarios, N., Duguet, T., Vahlas, C., Boudouvis, A.G., 2016. Multiscale modeling and experimental analysis of chemical vapor deposited aluminum films: linking reactor operating conditions with roughness evolution. Chem. Eng. Sci. 155, 449–458.

Aviziotis, I.G., Duguet, T., Vahlas, C., Boudouvis, A.G., 2017. Combined macro-/nano-scale investigation of the CVD of Fe from $Fe(CO)_5$. Adv. Mater. Interf. 1601185, 1–10.

Chaudhuri, S., Rangan, S., Veyan, J.-F., Muckerman, J.T., Chabal, Y.J., 2008. Formation and bonding of alane clusters on Al(111) surfaces studied by infrared absorption spectroscopy and theoretical modeling. J. Am. Chem. Soc. 130, 10576–10587.

Cheimarios, N., Kokkoris, G., Boudouvis, A.G., 2010. Multiscale modeling in chemical vapor deposition processes: coupling reactor scale with feature scale computations. Chem. Eng. Sci. 65, 5018–5028.

Choy, K.L., 2003. Chemical vapour deposition of coatings. Prog. Mater. Sci. 48, 57–170.

Deen, W.M., 1998. Analysis of transport phenomena. Oxford University Press, New York, USA.

Delmas, M., Poquillon, D., Kihn, Y., Vahlas, C., 2005. Al-Pt MOCVD coatings for the protection of Ti6242 alloy against oxidation at elevated temperature. Surf. Coat. Technol. 200, 1413–1417.

Frigo, D.M., van Eijden, G.J.M., Reuvers, P.J., Smit, C.J., 1994. Preparation and properties of alane dimethylethylamine, a liquid precursor for MOCVD. Chem. Mater. 6, 190–195.

Hamasha, M.H., Alzoubi, K., Switzer III, J.C., Lu, S., Desu, S.B., Poliks, M., 2011. A study on crack propagation and electrical resistance change of sputtered aluminium thin film on poly ethylene terephthalate substrate under stretching. Thin Solid Films 519, 7918–7924.

Han, J.S., Jensen, K.F., Senzaki, Y., Gladfelter, W.L., 1994. Pyrolytic laser assisted chemical vapor deposition of Al from dimethylethylamine-alane: Characterization and a new two-step writing process. Appl. Phys. Lett. 64, 425–427.

Hersee, S.D., Ballingal, J.M., 1990. The operation of metalorganic bubblers at reduced pressure. J. Vac. Sci. Technol. A 8, 800–804.

Jang, T.W., Moon, W., Baek, J.T., Ahn, B.T., 1998. Effect of temperature and substrate on the growth behaviors of chemical vapor deposited Al films with dimethylethylamine alane source. Thin Solid Films 333, 137–141.

Kawamura, H., Kumar, V., Sun, Q., Kawazoe, Y., 2003. Cyclic and linear polymeric structures of Al_nH_{3n} (n=3-7) molecules. Phys. Rev. A 67 (063205), 1–8.

Kim, B.-Y., Li, X., Rhee, S.-W., 1996. Microstructure and deposition rate of aluminum thin films from chemical vapor deposition with dimethylamine alane. Appl. Phys. Lett. 68, 3567–3569.

Kleijn, C.R., 2000. Computational modeling of transport phenomena and detailed chemistry in chemical vapor deposition – a benchmark solution. Thin Solid Films 365, 294–306.

Kleijn, C.R., Dorsman, R., Kuijlaars, K.J., Okkerse, M., van Santen, H., 2007. Multi-scale modeling of chemical vapor deposition processes for thin film technology. J. Cryst. Growth 303, 362–380.

Kuwana, K., Li, T., Saito, K., 2006. Gas-phase reactions during CVD synthesis of carbon nanotubes: Insights via numerical experiments. Chem. Eng. Sci. 61, 6718–6726.

Lee, H.M., Seo, J.Y., Jung, A., Choi, S.-Y., Ko, S.H., Jo, J., Park, S.B., Park, D., 2014. Longterm sustainable aluminum precursor solution for highly conductive thin films on rigid and flexible substrates. ACS Appl. Mater. Interf. 6, 15480–15487.

Letterman, R.D., Iyer, D.R., 1985. Modeling the effects of hydrolyzed aluminum and solution chemistry on flocculation kinetics. Environ. Sci. Technol. 19, 673–681.

Luo, B., Gladfelter, W.L., 2009. Chemical vapor deposition of metals: W, Al, Cu and Ru. In: Jones, A.C., Hitchman, M.L. (Eds.), Chemical Vapor Deposition: Precursors, Processes and Applications. Elsevier Ltd., Oxford, p. 329.

Masu, K., Yokoyama, M., Matsuhashi, H., Tsubouchi, K., 1994. Contribution of free electrons to Al CVD on a Si surface by photo-excitation. Appl. Surf. Sci. 79–80, 237–243.

Matsuhashi, H., Lee, C.-H., Nishimura, T., Masu, K., Tsubouchi, K., 1999. Superiority of DMAH to DMEAA for al CVD technology. Mater. Sci. Semicond. Process. 2, 303–308.

Michos, F.I., Sgouros, A.P., Sigalas, M.M., 2016. Ab initio study of boron and aluminum hydrides nanoparticles. Int. J. Hydrogen Energy 41, 20210–20216.

Nakajima, T., Nakatomi, M., Yamashita, K., 2003. Quantum chemical calculations on Al-CVD using DMEAA: surface reaction mechanism of AlH_3 on Al(111). Mol. Phys. 101, 267–276.

Robinson, D.W., Rogers Jr, J.W., 2000. Low temperature atomic layer growth of aluminum nitride on Si(100) using dimethylethylamine alane and 1,1-dimethylhydrazine. Thin Solid Films 372, 10.

Simmonds, M.G., Taupin, I., Gladfelter, W.L., 1994. Selective area chemical vapor deposition of aluminum using dimethylethylamine alane. Chem. Mater. 6, 935–942.

Sundman, B., Ohnuma, I., Dupin, N., Kattner, U.R., Fries, S.G., 2009. An assessment of the entire Al–Fe system including $D0_3$ ordering. Acta Mater. 57, 2896–2908.

Tan, C.M., Roy, A., 2007. Electromigration in ULSI interconnects. Mater. Sci. Eng. R Rep. 58, 1–75.

Vahlas, C., 2010. Chemical vapor deposition of metals: from unary systems to omplex metallic alloys. In: Belin-Ferré, E. (Ed.), Surface Properties and Engineering of Complex Intermetallics, Book Series on Complex Metallic Alloys, vol. 3. World Scientific, Singapore, pp. 49–81.

Xenidou, T.C., Boudouvis, A.G., Markatos, N.C., Samélor, D., Senocq, F., Prud'homme, N., Vahlas, C., 2007. An experimental and computational analysis of a MOCVD process for the growth of Al films using DMEAA. Surf. Coat. Technol. 201, 8868–8872.

Xenidou, T.C., Prudhomme, N., Vahlas, C., Markatos, N.C., Boudouvis, A.G., 2010. Reaction and transport interplay in Al MOCVD investigated through experiments and computational fluid dynamic analysis. J. Electrochem. Soc. 157, D633–D641.

Yun, J.-H., Kim, B.-Y., Rhee, S.-W., 1998a. Metal-organic chemical vapor deposition of aluminum from dimethylethylamine alane. Thin Solid Films 312, 259–264.

Yun, J.-H., Park, M.-Y., Rhee, S.-W., 1998b. Fourier transform infrared diagnostics of gas phase reactions in the metalorganic chemical vapor deposition of aluminum from dimethylethylamine alane. J. Vac. Sci. Technol. A 16, 419–423.